Design and Implementation of a Linear Active Disturbance Rejection Controller for Continuous Linear Motion of Multi-Span Center Pivot Systems

Bedri Bahtiyar* **and Şahin Sarikaya**

Department of Electrical and Electronics Engineering, Pamukkale University, Kinikli Campus, Camlaralti Neighbourhood, 20070 Denizli, Türkiye; bedribahtiyar@pau.edu.tr, ssarikaya101@posta.pau.edu.tr

* Correspondence author

Abstract: *This study presents a comparative analysis of Linear Active Disturbance Rejection Control (LADRC) and classical Proportional-Integral-Derivative (PID) control for managing the continuous linear motion of a multi-span center pivot irrigation system (MS-CPIS). A laboratory-scale prototype composed of three interconnected spans was developed to simulate real-world MS-CPISs. The control objective was to ensure synchronized and continuous motion among all spans while maintaining minimal angular deviation near 180° at the joints. Experimental evaluations were conducted under varying constant-speed scenarios, during which both tracking accuracy and control smoothness were taken into account. The smoothness of control inputs was quantified using the Integral of Squared Derivative (ISD), and tracking performance was evaluated by Root Mean Square Error (RMSE). The results show that LADRC produces significantly smoother control actions than the PID controller across all conditions while achieving comparable or superior tracking performance, especially after the transient phase. Additionally, LADRC showed advantages in ease of tuning and robustness against disturbances. These findings suggest that LADRC is a highly promising control strategy, for practical implementation in center pivot systems, offering enhanced precision, reliability and long-term operational efficiency.*

Keywords: Center Pivot Irrigation System, Linear ADRC, PID Control

1 Introduction

The negative effects of climate change and resource depletion require the adoption of more efficient irrigation strategies in agriculture [1]. To meet plant water needs optimally, these systems must distribute water evenly across the soil [2]. Center pivot irrigation systems (CPIS) stand out due to their efficiency, albeit their success heavily depends on the movement mechanism of their transport towers [3][4].

Traditional electric drives operate on a start-stop principle, directly affecting rotation speed and the volume of water applied [5]. When a tower stops, water or agrochemicals accumulate at specific points, significantly disrupting the growth balance of crops [6]. Movement irregularities in inner towers further degrade the uniformity of water distribution across the field [7]. Consequently, maintaining continuous span movement and strict tower alignment is critical to maximizing overall irrigation uniformity [8][9]. Furthermore, traditional start-stop operation causes mechanical fatigue, creating problems in chemical applications and reducing motor lifespan [10][11].

To compensate for water application errors, variable rate irrigation technologies utilizing solenoid valves were proposed [12]. However, the constant switching of these valves causes rapid wear and tear, negatively impacting overall cost-efficiency [13]. To overcome alignment problems proactively, advanced distributed and leader-follower collaborative navigation control methods based on RTK-GPS were developed [14][15]. Despite offering high precision, GNSS-based systems suffer from signal blockages in dense areas and challenging environmental conditions [16][17]. Since inaccurate position data can disrupt the consistent linear motion of the spans, continuous-turn linear potentiometers placed at the joints provide a more reliable and cost-effective measurement alternative.

The main motivation for this study stems from the fact that, although the continuous and linear movement of center pivot systems (CPS) is crucial for precision agriculture, existing studies on this topic remain highly localized and limited in number. Furthermore, the preferred methods for obtaining the joint angles required for control are often expensive and have various limitations. Therefore, the continuous development of control strategies focusing on uninterrupted motion is a priority to ensure the homogeneity of irrigation, spraying, and similar agricultural practices, thereby increasing overall productivity. In this study, a laboratory prototype that can be considered as the mechanical and electronic equivalent of a real 3-spanCPS was first constructed with joint angles measured using continuous-turn potentiometers. Control studies were conducted on this prototype in a laboratory environment to ensure continuous and linear motion of the CPS in various scenarios that a CPS operating in a real agricultural field might encounter. Since the mathematical model of a CPS includes uncertainty, which often represents the dominant dynamic effect in the system, LADRC was preferred for CPS control, as its superior performance under uncertain conditions has been demonstrated. To compare the control performance of the LADRC, the PID controller, which is frequently used in academic and industrial studies, was employed.

Alongside the advanced data-driven approaches recently highlighted in the literature, such as PI controller tuning via data-driven algorithms [18], robust fixed-point transformations [19], hybrid data-driven active disturbance rejection and sliding mode controls for crane systems [20][21], fractional-order direct adaptive fuzzy sliding mode control [22] and evolving neuro-fuzzy control frameworks [23], the LADRC proposed in this study serves as a highly practical alternative tailored for the specific needs of CPS. While these sophisticated methods have proven to be exceptionally successful in various complex mechatronic systems, their implementation generally requires comprehensive fuzzy rules, large training datasets, or high-capacity computational hardware. Driven by the motivation for wide accessibility in agricultural operations, LADRC's low computational burden enables seamless execution on standard, cost-effective microcontrollers. Its intuitive bandwidth-parameterization allows rapid, on-site calibration by field engineers. Mechanically, its theoretical capacity to generate smooth control outputs directly reduces actuator fatigue and extends motor lifespans, providing a robust and economical agricultural solution. Furthermore, the stability analysis of such data-driven and learning-based control systems remains a sensitive and critical topic, as stability is traditionally heavily reliant on exact models, which is comprehensively discussed in recent literature [24].

In addition, the effectiveness of active disturbance rejection was widely demonstrated in the broader context of higher-order model-free control. For instance, adaptive model-free sliding mode techniques [25] and high-order model-free predictive controls [26] have shown great success in handling extreme disturbances and unmodeled dynamics. However, since these high-order and predictive frameworks often demand substantial computational resources and complex algorithmic execution, the proposed second-order LADRC provides a much more practical, easy-to-tune and computationally lightweight alternative that can seamlessly operate on cost-effective microcontrollers for agricultural applications.

In order to demonstrate their performance in controlling the CPS prototype, the PID controller and LADRC were implemented on an easily accessible and inexpensive microcontroller board and real-time experiments were conducted. As a result of experimental studies, it was observed that LADRC is superior to the PID controller, especially in terms of steady-state behavior performance and smoothness of the control signal, even under disturbance effects. Thus, the contribution of this study to the literature is believed to be the proposal of the LADRC mechanism to ensure the continuous and linear movement of a CPS and the use of continuous rotation linear potentiometers placed at the joints as measurement devices within this feedback control structure.

The remainder of this paper is organized as follows. First, the CPS structure and the PID controller and LADRC used to control it are introduced. Experimental results on controlling the CPS with the PID controller and LADRC are then presented, and the performance of the controllers is compared. The final section includes a discussion and conclusions.

2 Problem Definition

In this section, the center pivot system will be introduced first, then the PID controller and the second-order linear ADRC used to ensure continuous and linear motion of the system will be explained. Before detailing the system models and controllers, the fundamental assumptions defining the scope of the controlled processes in this study are grouped as follows: First, although unpredictable disturbances render the physical system nonlinear, it is assumed that the system operates within a linear range once the spans begin to operate after being positioned to form a straight line. Second, for the LADRC formulation, it is assumed that the system input parameter b is unknown, but can be expressed as $b = b_0 + \Delta b$, assuming only that the approximate nominal value (b_0) is known while the rest (Δb) is treated as an unmodeled dynamics.

2.1 Center Pivot System

The center pivot system is a widely used irrigation mechanism designed to efficiently water large agricultural fields. It consists of a center fixed pivot point and a series of interconnected spans equipped with sprinklers that rotate around the pivot, forming a circular irrigation pattern. CPS is widely used due to its ability to provide uniform water distribution while optimizing resource usage, making it a preferred choice for large-scale farming operations.

The CPS's movement begins with the motor at the end of the outermost span rotating at a constant speed. From this point on, maintaining the linear alignment and continuous movement of the spans is critical to ensuring proper irrigation. However, environmental factors such as variable soil conditions, uneven terrain, mechanical degradation over time, and wind forces can cause unpredictable interruptions in the spans' ability to maintain continuous linear movement. The main challenge is to ensure the coordinated and uninterrupted movement of all spans under the influence of uncertain and dynamic external factors.

Basically, the dynamic model of each span can be presented as:

$$\begin{aligned} \dot{\theta}_i(t) &= \frac{r_i}{L_i}\omega_i(t) \\ \dot{\omega}_i(t) &= a_i\omega_i(t) + b_i u_i(t) d_i(t) \end{aligned} \quad (1)$$

where θ and ω represent the linear velocity relative to the center of the span and the angular velocity of the DC motor driving the span, respectively, while $i = 1,2,\ldots,M-1$ denotes the index of the span in a system consisting of M spans. In addition, r is the radius of the wheel attached to the span and L is the length of the span. The parameter a characterizes the damping effects within the system, while b quantifies the influence of the control input $u(t)$ on the dynamics of the system. The disturbance term $d(t)$ represents all the disturbance inputs that affect the system, and these effects are usually the most determining quantity in the model.

Although the mathematical model of the system can be obtained in this way with the geometric approach, due to the difficulty of determining these unpredictable disturbances, it is almost impossible to create a realistic, accurate and reliable mathematical model of the system. Therefore, the use of simulation models alone becomes almost impractical for representing the system dynamics with high fidelity.

Since the main purpose of this study is to ensure continuous and linear movement while performing operations such as irrigation and spraying, a laboratory prototype of the real-world 3-span CPS shown in Figure 1 was constructed. This prototype replicates the mechanical configuration and operational principles of a full-scale CPS, enabling experimental validation of control strategies under controlled conditions. The prototype consists of a center pivot connected to three spans. Each span is equipped with a DC motor that drives the wheels, corresponding motor drivers, and continuous-turn linear potentiometers to measure the joint angles. Each span is 30cm long, the height of the pivot and each linkage point is 10cm, and the diameter of each wheel is 4.5cm. Continuous-turn linear potentiometers provide real-time measurements of relative angles between spans, allowing precise observation of system kinematics and implementation of effective feedback control strategies. The DC motor connected to one of the two wheels in the mechanism at the end of the spans is driven by the PWM signal generated by the center control unit.

Figure 1
The prototype of CPS

The system begins by rotating the end motor at a constant speed. Then, during continuous motion, appropriate control signals are applied to the motors at the joints by local controllers located in the center control unit to align the inner spans to form a line between the center and the outer end and to maintain this position at all times. This aims to ensure continuous and linear motion of the 3-span CPS. Although the presence and estimated forms of the disturbances specified by d_i in Equation (1) render the system nonlinear, it can be assumed that the system operates within a linear range if the spans begin to operate after being positioned to form a straight line. Therefore, linear controllers were preferred.

2.2 PID Control

Traditional PID controllers remain the top choice in industrial settings due to their straightforward design, effectiveness, versatility, practicality, and ease of implementation [27][28]. Furthermore, their high adaptability ensures their continued successful application in resolving complex modern engineering challenges, such as the mitigation of nonlinear mechanical vibrations in rotary drilling systems [29]. A conventional PID controller can be approximated using numerical integration and differentiation methods. The discrete-time equivalent of the PID controller can be written in the following incremental form:

$$\begin{aligned} u[n+1] = u[n] + K_P(e[n] - e[n-1]) + K_I e[n] \\ + K_D(e[n] - 2e[n-1] + e[n-2]) \end{aligned} \tag{2}$$

where $u[n]$ is the control output at the discrete-time step n, $e[n]$ is the error at time step n, K_P is the proportional gain, K_I is the integral gain, and K_D is the derivative gain. This formulation allows the controller to be implemented efficiently in microcontrollers and real-time digital control systems by updating the control signal incrementally at each sampling instant.

Despite their widespread adoption, PID controllers, particularly for nonlinear systems, exhibit some limitations in managing system uncertainties and external disturbances. Given the inherent uncertainties in controlling the continuous, linear motion of a multi-span center pivot system, such as the large-amplitude disturbances to which the system is subjected, several limitations in PID controller performance are inevitable.

2.3 Linear Active Disturbance Rejection Control

LADRC is a highly effective control mechanism for systems subject to large-amplitude, uncertain disturbances, such as CPS. The foundational concept of active disturbance rejection was originally introduced by Han [30]. Subsequently, this structure was practically parameterized via bandwidth tuning by Gao, making it highly accessible for engineering applications [31]. Building upon these foundations, the method was successfully adapted to provide novel motion control design approaches [32] and effective tuning methods specifically tailored for second-order systems [33]. Furthermore, its overall superiority over traditional PID control was clearly demonstrated in various real-time industrial applications, such as high-precision positioning systems [34].

The tuning method proposed by Gao [31], which relies on the controller bandwidth ω_c and the damping ratio ξ, is defined as follows:

Consider the plant dynamics of a second-order system as:

$$\begin{aligned}\dot{x}_1(t) &= x_2(t)\\ \dot{x}_2(t) &= f\big(x_1(t), x_2(t)\big) + bu(t) + d(t)\\ &= f\big(x_1(t), x_2(t)\big) + b_0u(t) + \Delta b_0u(t) + d(t)\\ y(t) &= x_1(t)\end{aligned} \tag{3}$$

where $x_1(t)$, $x_2(t) \in \mathcal{R}^2$ are states, $u(t) \in \mathcal{R}$ is the input, $y(t) \in \mathcal{R}$ is the output of the system and $d(t) \in \mathcal{R}$ is the external disturbance. The internal dynamics of the system are represented by $f(x_1(t), x_2(t))$.

While LADRC is frequently classified as a data-driven approach, the design of its Extended State Observer (ESO) partially relies on structural plant knowledge, such as the system order and the nominal input gain b_0. However, its true data-driven nature lies in its ability to utilize real-time input-output data to dynamically estimate and compensate for unmodeled dynamics and external disturbances without requiring precise analytical models.

To achieve this, the internal system dynamics, modeling errors, and external disturbances present in Equation (3) are grouped into a single unified term known as the "total disturbance", defined as $D(t) = f\big(x_1(t), x_2(t)\big) + \Delta b_0u(t) + d(t)$. By treating this total disturbance as a newly introduced third state variable ($x_3(t) = D(t)$), the original second-order plant is expanded into the following third-order augmented state-space model:

$$\begin{aligned}\dot{x}_1(t) &= x_2(t)\\ \dot{x}_2(t) &= x_3 + b_0u(t)\\ \dot{x}_3(t) &= \dot{D}(t)\end{aligned} \tag{4}$$

Based on this augmented model, an ESO can be directly formulated to simultaneously estimate all three system states in real-time, capturing both the physical kinematics and the total disturbance, as follows:

$$\begin{aligned}\dot{z}_1(t) &= z_2(t) + l_1\big(y(t) - z_1(t)\big)\\ \dot{z}_2(t) &= z_3 + b_0u(t) + l_2\big(y(t) - z_1(t)\big)\\ \dot{z}_3(t) &= l_3\big(y(t) - z_1(t)\big)\end{aligned} \tag{5}$$

Here, z_1, z_2 and z_3 are estimated states of system output, velocity, and total disturbance, respectively, and l_1, l_2 and l_3 are the observer gains. Then, the control law can be expressed as:

$$u = \frac{1}{b_0}\big(K_p(r - z_1) - K_d z_2 - z_3\big) \tag{6}$$

where r is the set point and K_p and K_d are the proportional gain and the derivative gain, respectively, similar to that of a PID controller. These gains of the LADRC can be obtained as follows:

$$K_p = (\omega_c)^2, K_d = 2\xi\omega_c \tag{7}$$

where ω_c and ξ are natural frequency and damping ratio of the controller, respectively. Then,

$$\omega_o \approx (3 \dots 5)\omega_c \tag{8}$$

is defined to obtain the gains of the ESO that will be computed as:

$$l_1 = 3\omega_o, l_2 = 3\omega_o^2, l_3 = w_o^3 \tag{9}$$

Figure 2 illustrates the closed-loop system controlled by LADRC. The reference $r(t)$ is processed by the LADRC controller. The controller computes the control signal $u(t)$ using estimated states. The plant receives $u(t)$ and generates the output $y(t)$. The ESO estimates $x_1(t)$, $x_2(t)$ and $x_3(t)$ from the system output $y(t)$ for the applied input signal $u(t)$. The estimated states are used to compensate for disturbances and improve tracking.

While the theoretical framework of LADRC and its Extended State Observer (ESO) is presented in continuous time for mathematical clarity, its digital implementation on the center microcontroller operates in discrete time. The specific discretization techniques bridging this theoretical-practical gap, such as the application of the fourth-order Runge-Kutta (RK4) method for the ESO, are detailed in the subsequent experimental results section.

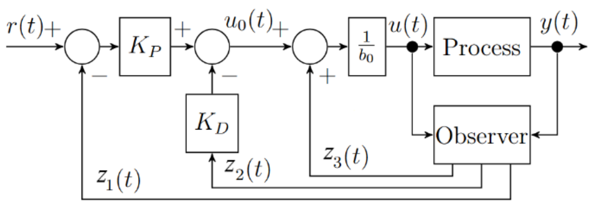

Figure 2

Closed-loop structure controlled by LADRC

3 Experimental Results

The 3-span CPS is a Multi-Input Multi-Output (MIMO) system comprising two control inputs and two measured outputs. Each span is driven by an individual DC motor, with the actuation forces denoted by τ_1 , τ_2 whereas, τ_3 serves as the reference input illustrated in Figure 3. The system is equipped with two continuous-turn linear potentiometers positioned at the joints between Span 1 and Span 2, and between Span 2 and Span 3, denoted as θ_{12} and θ_{23} respectively. These sensors provide real-time measurements of the relative angles at the joints.

The purpose of the control system is to ensure that all spans move in a near-linear formation, following the initiation of the outer motor, which operates at a constant speed defined by the reference input $r_3 = \tau_3$. To achieve this objective, the controller must generate the appropriate torques $u_1 = \tau_1$ and $u_2 = \tau_2$ such that the joint angles $y_1 = \theta_{12}$ and $y_2 = \theta_{23}$ are both 180°. This 3-span CPS is essentially a MIMO system, but near the equilibrium point, all spans move almost like a straight line and under these conditions, the system can be considered as two separate Single-Input Single-Output (SISO) systems, as each span has its own unique input that must be manipulated to keep its output at 180°.

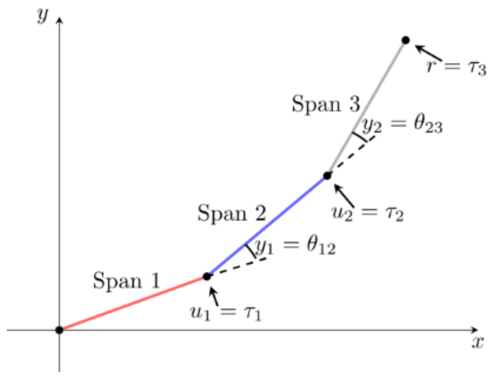

Figure 3
The geometric presentation of the three-span CPS

The block diagram of the control system is shown in Figure 4. The center control unit is implemented using the NuMaker-PFM-M487 development board, which features the M487JIDAE microcontroller based on the ARM Cortex-M4F architecture. Spans are denoted as "Span 1", "Span 2" and "Span 3" from the innermost to the outermost, respectively. Each span is equipped with a motor driver (D_i) and a corresponding DC motor (M_i). Furthermore, linear potentiometers (R_1, R_2) are installed at the joints between adjacent spans, with the exception of the outermost span. Acting as voltage dividers, these potentiometers serve as angle sensors, providing voltage signals that correspond to the angular variations at the joints caused by the rotation of the spans. The voltages obtained from the angle sensors at the joints are applied to the corresponding ADC inputs of the microcontroller. The digital outputs of the ADC conversions are then processed to calculate the actual angles on each joint, which are denoted by θ_{12}, θ_{23}. After the movement of the outermost span is started at a constant angular velocity $r_3 = \tau_3$, the controllers (C_1 and C_2) generate suitable control inputs (u_1, u_2) that are applied to the driver of each span as PWM signals, ensuring that the angles at all joints remain at 180°.

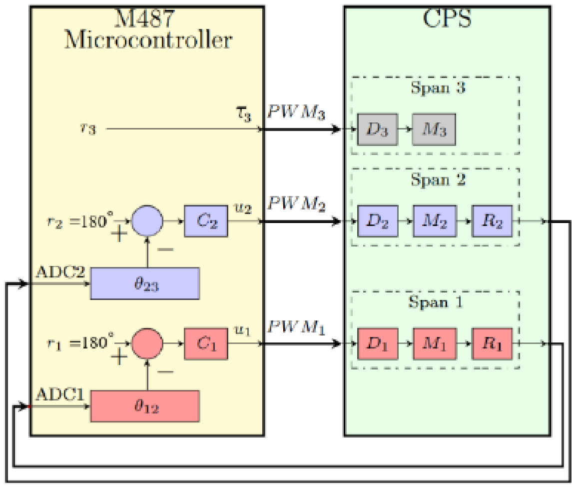

Figure 4
Block diagram of the control system

Real-time experiments were conducted to evaluate the performance of the controllers, where both the control period and the controller parameters were determined experimentally. The M487 microcontroller operates at 192MHz, with control timing managed through a timer interrupt. The step response of the outermost DC motor showed that both the sampling period and the control period could be set to $t = 1$ms during the experiments. Upon each interrupt, the precomputed control signals $u_1(t)$, $u_2(t)$, implemented as PWM outputs, were applied to the system inputs. After applying these signals, the voltage readings from the ADCs, corresponding to the angle of each joint, were converted into angle values and fed back to the controller to compute the next control input. The conversion of ADC readings into angular positions and all control computations were implemented using the M487's floating-point library, which utilizes single-precision arithmetic to effectively reduce rounding errors and enhance computational efficiency.

During preliminary tests, it was observed that variations in the initial joint angles significantly affected the transient response time required to achieve the desired linear position, subsequently causing substantial differences in both the overall RMSE and ISD metrics. Therefore, to ensure a perfectly fair comparison between the controllers across all different scenarios, identical initial conditions were established for every experimental run. Before initiating each test, all spans were physically aligned against a predefined starting boundary line, ensuring that the system always started from a consistent, stationary configuration.

During the experiments, the performance of the controllers was investigated in three distinct control scenarios, each corresponding to a different constant speed of the outermost motor. These scenarios were defined by setting the PWM duty cycles to 50%, 75%, and 100%, respectively. It was observed that slight modifications to the controller parameters were necessary as the operating conditions changed between scenarios. Therefore, the controller parameters for both controller types were initially tuned in the second scenario (75% PWM duty cycle). Thus, the same parameters were subsequently employed without further adjustment for the first (50% PWM duty cycle) and third (100% PWM duty cycle) scenarios. In addition, obstacles in the form of steep drop-off ramps were placed at three different locations along the CPS trajectory, creating a disturbance effect. These steep drop-off ramps were explicitly designed to emulate severe, highly nonlinear agricultural disturbances such as deep tire ruts or sudden soil subsidence. Such large-amplitude disruptions introduce complex, unmodeled transient dynamics into the system. This challenging environment thoroughly justifies the necessity and effectiveness of the data-driven LADRC approach, as simple linear or traditional model-based controllers struggle to maintain stability under these severe conditions. Specifically, the first obstacle was positioned to disturb only Joint 1, the second to disturb only Joint 2, and the third to simultaneously disturb both joints. The controller parameters were adjusted considering tracking error (RMSE) and control input variation (ISD), which are formally imposed as the performance specifications. To satisfy these specifications, an empirical grid search was utilized, acting as an experimental multi-objective optimization problem aimed at minimizing both metrics. Furthermore, the parameters of the two controllers used for each joint were chosen to be the same.

To ensure a fair comparison, both controllers were tuned empirically based on real-time experimental data rather than relying on precise analytical models. While analytical approaches such as the Extended Symmetrical Optimum method offer convenient tuning to achieve an optimal trade-off among performance indices [37], an empirical grid search was explicitly utilized in this study to determine the PID controller parameters, where the search spaces for K_P and K_I were defined over the range $[0.1, 30.0]$ with a step size of 0.5, while the search space for K_D was defined in the range $[0.1, 1.0]$ and a step size of 0.1. This exhaustive empirical search yielded the optimal parameters: $K_P = 15$, $K_I = 8$, and $K_D = 0.5$. Experimental results showed that neighboring values within the search grids did not provide significantly different control performance. Consequently, the final controller parameters were selected without considering small decimal differences, rounding to the nearest integer for K_P and K_I, and to the nearest tenth for K_D. The parameters adjusted during the second scenario were then applied to the first and third scenarios without any modification.

On the other hand, the second-order LADRC parameters, as defined in Equations (7) and (9), were also determined by an experimental grid search. To facilitate the tuning process, the parameter b_0 was initially set to 1. Based on this assumption, a grid search was performed to determine the optimal controller bandwidth ω_c, evaluated over the interval $[0.25, 10]$ with a step size of 0.25, while damping ratio

ξ is set to 0.6. After defining the optimum ω_c, a secondary grid search was conducted for ξ over the interval [0.1,1.2] with a step size of 0.1. Based on the experimental results, the most suitable ω_c and ξ for the two LADRCs were found to be $\omega_c = 4.5$ and $\xi = 0.6$, resulting in gains in controller and observer of $K_p = 20.25$, $K_d = 5.4$, $l_1 = 40.5$, $l_2 = 546.75$ and $l_3 = 2460.375$. Furthermore, the scaling factor linking the observer bandwidth to the controller bandwidth, defined within the range [3,5] in Equation (8), was selected as 3. It should be noted that the Extended State Observer, defined in Equation (5), was implemented in discrete time using the fourth-order Runge-Kutta (RK4) method.

The performance of both controllers on joint angle trajectories and control inputs in each control scenario are presented in Figures 5-10. To facilitate comparison, the PID controller and LADRC results for each scenario are shown consecutively. The inset plots within the joint angle graphs provide a magnified view of the angular deviations as the CPS encounters the first, second, and third obstacles, respectively. These plots reveal that the LADRC exhibits superior tracking performance, characterized by a significantly smaller overshoot in response to disturbances than the PID controller.

During the experiments, it was observed that the parameters of the LADRC structure were significantly more straightforward to tune than those of the PID controller, particularly when the control objective prioritized smooth control efforts to enhance overall performance. This feature provided a significant advantage for the on-site calibration of individual joint controllers in full-scale agricultural center pivot systems.

In addition to evaluating the tracking performance, the smoothness of the control inputs was also taken into consideration, since it plays a critical role in preserving actuator lifetime and enhancing energy efficiency. To quantify these objectives, the control results at each joint during the experiment were analyzed through two performance metrics. First, to evaluate the smoothness of the control signal, the Integral of Squared Derivative (ISD) of the control input was computed as follows:

$$\text{ISD} = \sum_{n=2}^{N} \left(\frac{u[n] - u[n-1]}{\Delta t} \right)^2 \Delta t \quad (10)$$

where Δt represents the sampling time interval. Second, to evaluate the tracking performance, the root mean square error of the joint angles expressed in degrees was calculated as:

$$RMSE = \sqrt{\frac{1}{N} \sum_{n=1}^{N} e[n]^2} \quad (11)$$

Here, the tracking error was defined as $e[n] = 180° - y[n]$, where $y[n]$ was the angle value at the joints and N represented the number of data samples.

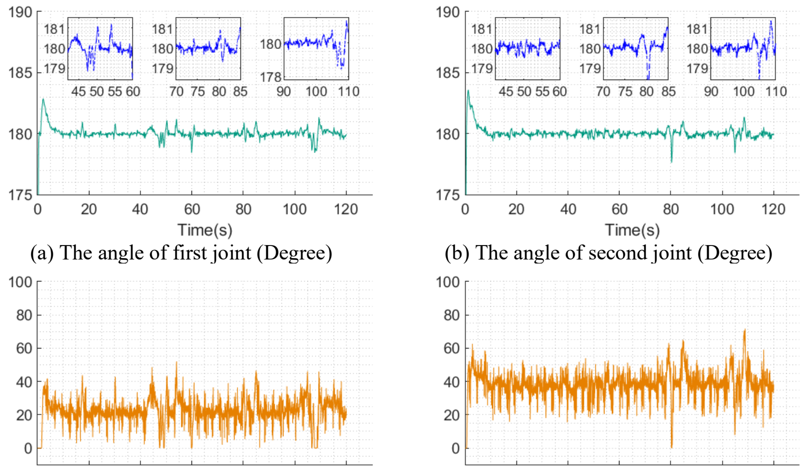

(a) The angle of first joint (Degree)

(b) The angle of second joint (Degree)

(c) The control signal for the first motor (PWM)

(d) The control signal for the second motor (PWM)

Figure 5
The PID control results for scenario 1

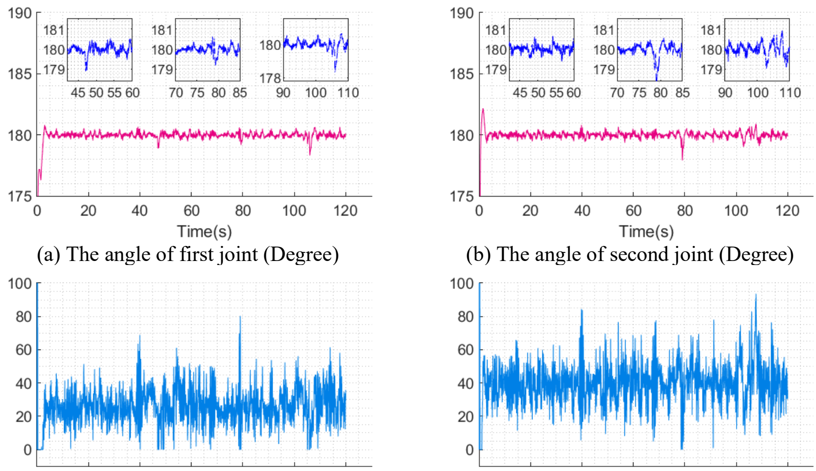

(a) The angle of first joint (Degree)

(b) The angle of second joint (Degree)

(c) The control signal for the first motor (PWM)

(d) The control signal for the second motor (PWM)

Figure 6
The LADRC results for scenario 1

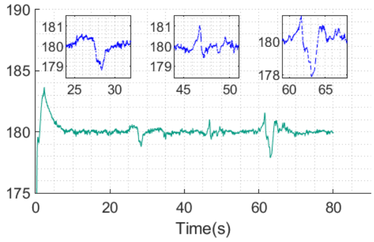

(a) The angle of first joint (Degree)

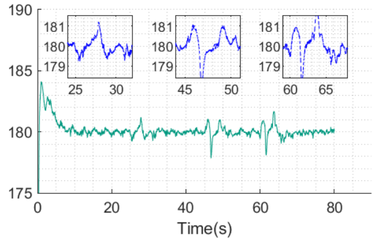

(b) The angle of second joint (Degree)

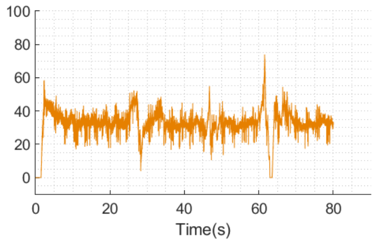

(c) The control signal for the first motor (PWM)

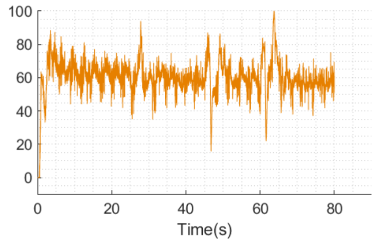

(d) The control signal for the second motor (PWM)

Figure 7
The PID results for scenario 2

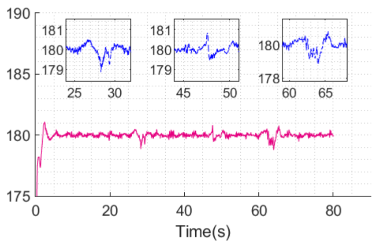

(a) The angle of first joint (Degree)

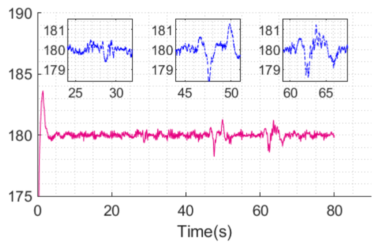

(b) The angle of second joint (Degree)

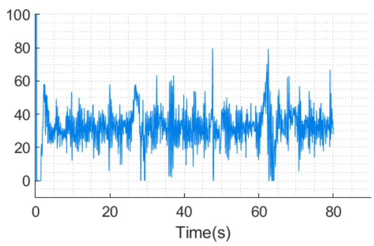

(c) The control signal for the first motor (PWM)

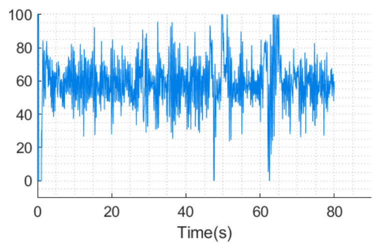

(d) The control signal for the second motor (PWM)

Figure 8
The LADRC results for scenario 2

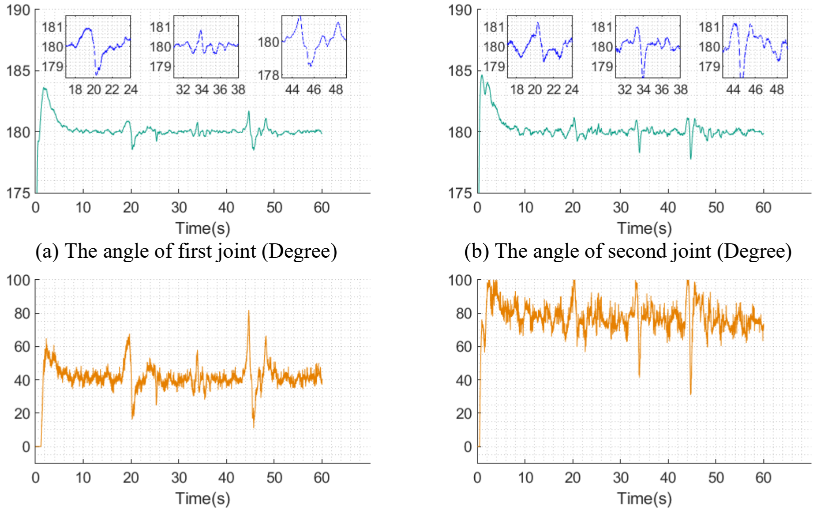

(a) The angle of first joint (Degree)

(b) The angle of second joint (Degree)

(c) The control signal for the first motor (PWM)

(d) The control signal for the second motor (PWM)

Figure 9
The PID results for scenario 3

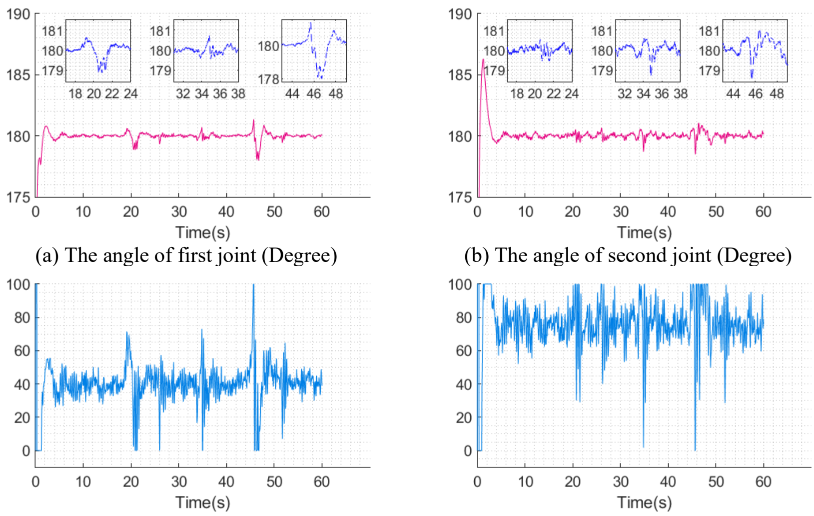

(a) The angle of first joint (Degree)

(b) The angle of second joint (Degree)

(c) The control signal for the first motor (PWM)

(d) The control signal for the second motor (PWM)

Figure 10
The LADRC results for scenario 3

Experimental results demonstrated that the LADRC produced significantly lower ISD values compared to the PID controller, indicating smoother control efforts with fewer abrupt variations. However, in terms of RMSE, the PID controller demonstrated slightly better tracking performance when evaluated over the entire experimental duration. These findings show that, while LADRC effectively suppressed control signal fluctuations, its initial transient response characteristics likely contributed to a marginally higher overall tracking error. A comprehensive summary of these results is provided in Table 1.

To better evaluate the steady-state behavior of the controllers, a second analysis was performed using the data collected after $t = 10$s. At this stage, both controllers can be considered to have reached steady-state operation, and for LADRC, this implies that the ESO has sufficiently converged. In the period following $t = 10$s, the LADRC clearly demonstrated clear superiority over the PID in both ISD and RMSE. The significantly lower ISD values highlight the LADRC's ability to consistently produce smoother control efforts, while the difference in RMSE indicates improved tracking performance. These results confirm that the LADRC achieves both superior signal smoothness and tracking accuracy compared to the PID when the observer dynamics stabilize. Detailed results of this steady-state analysis are presented in Table 2.

Table 1
Performance comparison over the entire duration for all scenarios.

	Method	ISD u_1	ISD u_2	RMSE e_1	RMSE e_2
Scenario 1	PID	**3168.30**	15872.30	**1233.31**	**1239.87**
	LADRC	3649.16	**3802.82**	1249.89	1246.51
Scenario 2	PID	14022.21	15813.82	1238.98	**1244.83**
	LADRC	**3551.94**	**3480.86**	**1238.89**	1252.51
Scenario 3	PID	7287.31	8671.66	**1240.78**	**1250.47**
	LADRC	**3013.82**	**3067.34**	1241.21	1254.35

Table 2
Performance comparison after $t = 10$ seconds for all scenarios.

	Method	ISD u_1	ISD u_2	RMSE e_1	RMSE e_2
Scenario 1	PID	12703.58	15302.97	99.73	88.02
	LADRC	**2171.85**	**2456.29**	**71.21**	**77.50**
Scenario 2	PID	12898.18	14446.67	84.71	90.97
	LADRC	**1714.46**	**2095.84**	**52.23**	**69.91**
Scenario 3	PID	6536.63	7799.74	73.84	78.81
	LADRC	**1057.45**	**1374.38**	**67.03**	**56.27**

3 Discussion and Conclusions

This study proposes the use of an LADRC structure to ensure linear and continuous motion of center-pivot irrigation mechanisms, and continuous-rotation potentiometers to measure angular changes at the joints. To this end, a laboratory prototype of a center-pivot irrigation system was first constructed as a representative model of the center-pivot irrigation mechanism. Then, to simulate real-world operating conditions, real-time experimental control studies were conducted to ensure linear and continuous motion of the prototype under three different scenarios and in a test area with obstacles placed at three different points. While ensuring continuous linear motion of the CPIS for proper irrigation in agricultural fields is critical for the long-term operation of the system, protecting the mechanical and electronic systems and ensuring energy efficiency are equally important. Therefore, both tracking error and variations in control input were considered in the real-time control experiments conducted on the prototype.

The performance of the proposed LADRC structure was compared with the performance of the PID controller that is frequently preferred in the literature. The controllers were implemented on the low-cost and readily available Nuvoton-M487 microcontroller. To demonstrate the control performance of the two controller structures, a comparative evaluation was conducted using the RMSE values of the tracking errors and the ISD values of the control inputs. The overall experimental findings clearly demonstrated that the LADRC provided superior control performance, particularly during the steady-state period and under sudden disturbances. During the initial transient response of the experiment, the ESO within the LADRC converged to the actual system conditions within approximately 10 seconds. Afterward, the LADRC exhibited smoother control signals and lower tracking errors compared to the PID controller. These findings are presented both visually (graphs) and numerically in the tables.

Compared to recent works relying on complex network structures and costly RTK-GPS, this study introduces distinct new design features by embedding the empirically tuned LADRC into a standard microcontroller and utilizing continuous-turn potentiometers. These features offer a highly practical, easy-to-tune alternative to model-dependent and GNSS-based approaches, entirely eliminating satellite signal vulnerabilities.

Consequently, our results demonstrate that LADRC provides higher steady-state performance, lower mechanical stress, and higher energy efficiency in center pivot irrigation systems. Therefore, the proposed system is demonstrated to be a highly viable and robust solution for controlling center pivot systems used in irrigation, spraying, fertilizing and other applications in real-world agricultural environments, where robustness, adaptability and operational efficiency are crucial.

Acknowledgement

This work was not supported by any institution.

References

[1] Demir, A., Yılmaz, B., & Kaya, C. (2023). Modern irrigation strategies for sustainable agriculture. *Agricultural Water Management, 250*, 100967.

[2] Zhang, X., Wang, D., & Yao, R. (2013). Water application uniformity under center pivot irrigation systems. *Irrigation Science, 31(2)*, 131–139.

[3] O'Brien, D. M., Rogers, D. H., & Clark, G. A. (1998). Center pivot irrigation systems: Design and efficiency. Kansas State University Agricultural Experiment Station and Cooperative Extension Service Bulletin, MF-2246.

[4] Fusco, G. (1995). The effect of tower movement on irrigation uniformity in center pivot systems. *Irrigation and Drainage Systems, 9(3)*, 231–243.

[5] New, L. & Fipps, G. (1976). Center Pivot Irrigation. The OAKTrust Digital Repository. https://oaktrust.library.tamu.edu/server/api/core/bitstreams/fa006708-3400-40b0-a7c0-b28ec37312ba/content, (accessed: 05/04/2026)

[6] Tambo, J. A., Wünscher, T., & Mockshell, J. (2022). Chemical application challenges in precision irrigation systems. *Agricultural Water Management, 260*, 107251.

[7] Hanson, B. R., & Wallender, W. W. (1986). Bidirectional uniformity of water applied by continuous-move sprinkler machines. *Transactions of the ASAE, 29(4)*, 1047-1053.

[8] Fangmeier, D. D., Vlotman, W. F., & Eftekharzadeh, S. (1990). Uniformity of LEPA irrigation systems with furrow drops. *Transactions of the ASAE, 33(6)*, 1907-1912.

[9] Ouazaa, S., Bouksila, F., & Berndtsson, R. (2015). Impact of tower alignment on center pivot irrigation performance. *Irrigation Science, 33(2)*, 135–145.

[10] Evans, R. G. (2001). Center pivot irrigation systems: Hydraulic vs. electric drives. *Irrigation Science, 20(3)*, 159–168.

[11] Peters, T. R., Nelson, R. G., & Brooker, D. B. (2020). Effects of start-stop motion on motor life and irrigation uniformity in center pivot systems. *Applied Engineering in Agriculture, 36(3)*, 383–392.

[12] Chávez, J. L., Pierce, F. J., & Evans, R. G. (2010). Compensating inherent linear move water application errors using a variable rate irrigation system. *Irrigation Science, 28(3)*, 203-210.

[13] León Mostacero, J. A., Flores Magdaleno, H., & Ascensio Hernández, R. (2012). Implementación de riego a precisión en un sistema de pivote central. *Revista mexicana de ciencias agrícolas, 3(SPE4)*, 705-718

[14] Meng, F., Zhou, Y., & Zhang, H. (2022). Leader-follower collaborative navigation control for linear and center pivot irrigation systems. *Biosystems Engineering, 213*, 198–210.

[15] Meng, F., Zhou, Y., & Zhang, H. (2021). Distributed collaborative navigation control for multi-span irrigation machines. *Computers and Electronics in Agriculture, 186*, 106206.

[16] Fredeluces, J., Morales, R., & Brown, T. (2024). Challenges in GNSS positioning for precision agriculture. *Precision Agriculture, 25(1)*, 45–67.

[17] Mekik, Ç., & Arslanoğlu, M. (2009). GNSS applications in agriculture and future prospects. *Journal of Agricultural Sciences, 15(4)*, 389–397.

[18] Roman, R.-C., Precup, R.-E., Preitl, S., Szedlak-Stinean, A.-I., Bojan-Dragos, C.-A., Hedrea, E.-L., & Petriu, E. M. (2022). PI controller tuning via data-driven algorithms for shape memory alloy systems. *IFAC-PapersOnLine*, *55*(40), 181–186.

[19] Varga, B., Horváth, R., & Tar, J. K. (2025). Improved adaptation speed of the robust fixed point transformation-based controller using virtual response forecast. *Acta Polytechnica Hungarica*, *22*(3), 121–143.

[20] Roman, R.-C., Precup, R.-E., Petriu, E. M., & Borlea, A.-I. (2024). Hybrid data-driven active disturbance rejection sliding mode control with tower crane systems validation. *Romanian Journal of Information Science and Technology*, *27*(1), 50–64.

[21] Roman, R.-C., Precup, R.-E., & Petriu, E. M. (2024). Active disturbance rejection control for 3D crane systems. *Procedia Computer Science*, *242*, 976–983.

[22] He, D., Wang, H., Tian, Y., Zha, M., & Precup, R.-E. (2026). Fractional-order ultra-local model-based direct adaptive fuzzy sliding mode control for mechatronic systems with mismatched disturbances and input nonlinearities. *Fuzzy Sets and Systems*, *526*, 109674.

[23] Andonovski, G., Leite, D., Precup, R.-E., Gomide, F. A. C., Pratama, M., & Škrjanc, I. (2026). Advancements in data-driven evolving fuzzy and neuro-fuzzy control: A comprehensive survey. *Applied Soft Computing*, 114058.

[24] Precup, R.-E., Roman, R.-C., Hedrea, E.-L., Szedlak-Stinean, A.-I., & Zamfirache, I.A. (2025). Classical and Modern Optimization Techniques Applied to Control and Modeling (1st ed.). CRC Press.

[25] Liu, J., Zhong, H., Wang, Z., Jiang, X., Chen, Y., Gu, D., ... & Liu, L. (2026). Adaptive Model-Free Sliding Mode Fault-Tolerant Speed-Current Control for

Permanent Magnet Synchronous Motor under Extreme Operating Conditions with Parameters Mismatch. *Progress in Electromagnetics Research C*, *165*.

[26] Wei, Y., Chen, Y., Xie, H., Ke, D., & Wang, F. (2025). High-Order ARX-Based Model-Free Predictive Control on PMSM Drives with Hybrid Estimation. In *2025 IEEE Transportation Electrification Conference and Expo, Asia-Pacific (ITEC Asia-Pacific),* 1-6.

[27] Åström, K. J., & Hägglund, T. (1995). PID controllers: theory, design, and tuning. ISA-The Instrumentation, Systems and Automation Society.

[28] Ang, K. H., Chong, G., & Li, Y. (2005). PID control system analysis, design, and technology. *IEEE Transactions on Control Systems Technology, 13(4)*, 559–576.

[29] Tellaa, M., Aibeche, A., Doghmane, Z. M. & Kidouche, M. (2025). Stick-Slip Vibration Mitigation in Rotary Drilling Systems Using a Particle Swarm Optimization-based PID Controller under Varying Weight on Bit Conditions *ACTA POLYTECHNICA HUNGARICA, 22(9)*, 31-50

[30] Han, J. (1998). Active disturbance rejection control technique. *Control and Decision, 13(1)*, 19–23.

[31] Gao, Z. (2003). Scaling and bandwidth-parameterization based controller tuning. *Proceedings of the American Control Conference, 6*, 4989–4996.

[32] Gao, Z., Huang, Y., & Han, J. (2002). A novel motion control design approach based on active disturbance rejection. *Proceedings of the IEEE International Conference on Decision and Control*, 4877–4882.

[33] Chen, X., Li, D., Gao, Z., & Wang, C. (2011). Tuning method for second-order active disturbance rejection control. *Proceedings of the 30th Chinese Control Conference*, Yantai, China.

[34] Zheng, H., Tan, W., & Wang, H. (2016). Comparison of PID and LADRC control for a high precision positioning system. *International Journal of Control, Automation and Systems, 14(5)*, 1206–1215.

[35] Li, S., & Zheng, Y. (2019). Application of LADRC in industrial robotic motion control. *IEEE Transactions on Industrial Electronics, 66(8)*, 6093–6103.

[36] Wang, L., Zhou, Y., & Liu, X. (2021). Real-time implementation of LADRC for water level control systems. *Journal of Process Control, 103*, 112–124.

[37] Precup, R.-E., & Preitl, S. (1996). On the extended symmetrical optimum method. *Buletinul Stiintific al Universitatii Politehnica din Timisoara, Seria Automatica si Calculatoare*, 41(55), 15-22.